BAMS Article

The ARM Radar Network

At the Leading Edge of Cloud and Precipitation Observations

P. Kollias, N. Bharadwaj, E. E. Clothiaux, K. Lamer, M. Oue, J. Hardin, B. Isom, I. Lindenmaier, A. Matthews, E. P. Luke, S. E. Giangrande, K. Johnson, S. Collis, J. Comstock, and J. H. Mather

ABSTRACT: Improving our ability to predict future weather and climate conditions is strongly linked to achieving significant advancements in our understanding of cloud and precipitation processes. Observations are critical to making these advancements because they both improve our understanding of these processes and provide constraints on numerical models. Historically, instruments for observing cloud properties have limited cloud–aerosol investigations to a small subset of cloud-process interactions. To address these challenges, the last decade has seen the U.S. DOE ARM facility significantly upgrade and expand its surveillance radar capabilities toward providing holistic and multiscale observations of clouds and precipitation. These upgrades include radars that operate at four frequency bands covering a wide range of scattering regimes, improving upon the information contained in earlier ARM observations. The traditional ARM emphasis on the vertical column is maintained, providing more comprehensive, calibrated, and multiparametric measurements of clouds and precipitation. In addition, the ARM radar network now features multiple scanning dual-polarization Doppler radars to exploit polarimetric and multi-Doppler capabilities that provide a wealth of information on storm microphysics and dynamics under a wide range of conditions. Although the diversity in wavelengths and detection capabilities are unprecedented, there is still considerable work ahead before the full potential of these radar advancements is realized. This includes synergy with other observations, improved forward and inverse modeling methods, and well-designed data–model integration methods. The overarching goal is to provide a comprehensive characterization of a complete volume of the cloudy atmosphere and to act as a natural laboratory for the study of cloud processes.

https://doi.org/10.1175/BAMS-D-18-0288.1
Corresponding author: Pavlos Kollias, pavlos.kollias@stonybrook.edu
In final form 15 December 2019
©2020 American Meteorological Society
For information regarding reuse of this content and general copyright information, consult the AMS Copyright Policy.

AFFILIATIONS: Kollias—Stony Brook University, State University of New York, Stony Brook, and Brookhaven National Laboratory, Upton, New York, and University of Cologne, Cologne, Germany; **Bharadwaj,* Hardin, Isom, Lindenmaier, Matthews, Comstock, and Mather**—Pacific Northwest National Laboratory, Richland, Washington; **Clothiaux**—The Pennsylvania State University, University Park, Pennsylvania; **Lamer***—City College of New York, New York, New York; **Oue**—Stony Brook University, State University of New York, Stony Brook, New York; **Luke, Giangrande, and Johnson**—Brookhaven National Laboratory, Upton, New York; **Collis**—Argonne National Laboratory, Argonne, Illinois
* **CURRENT AFFILIATIONS: Bharadwaj**—Fortem Technologies, Pleasant Grove, Utah; **Lamer**—Brookhaven National Laboratory, Upton New York

The U.S. Department of Energy (DOE) Atmospheric Radiation Measurement (ARM) facility is the first organized effort to establish continuously operating surface-based observatories for atmospheric studies (Ackerman et al. 2016; Mather and Voyles 2013). During its early phase (1992–2009), the ARM observatories mostly focused on column (profiling) measurements of radiation, aerosols, and clouds. Each of the ARM observatories included a profiling millimeter-wavelength cloud radar (Kollias et al. 2005, 2016; Moran et al. 1998). In parallel, Europe established a number of atmospheric profiling observatories and established formal collaborations with the DOE ARM program (Haeffelin et al. 2016; Illingworth et al. 2007). Since 2009, ARM, propelled by a series of science workshop recommendations, embarked on a considerable expansion of its observing capabilities. The scientific drivers for the ARM radar network expansion included advancing the documentation of the life cycle of clouds over previous column observations, better characterizing the mesoscale organization of clouds and precipitation, improving microphysical retrievals, and extending the ARM observations to precipitating clouds and deep convection.

The requirement to detect both small and large hydrometeors and their associated cloud and precipitation systems over a large domain, necessitated ARM to overcome radar community barriers (weather vs cloud radar users and applications) and pioneered the first, systematic, large-scale, symbiosis of centimeter- and millimeter-wavelength radars at its observatories (Fig. 1). Earlier examples of symbiosis of cm- and mm-wavelength radars include the National Center for Atmospheric Research S-Pol and Ka-band (SPolKa; Ellis and Vivekanandan 2011) radar system and efforts in research universities (Hogan and Goddard 1999; Kollias et al. 2003). Historically, centimeter-wavelength radars had been used to observe and characterize the bulk properties of hydrometeors in precipitation for over 50 years (Bringi and Chandrasekar 2001; Doviak and Zrnić 1993). Centimeter-wavelength radar systems were used both for research and monitoring of precipitation

Fig. 1. DOE ARM past, present, and planned deployments as of March 2019. The ARM program has been deploying radars and other instruments to its fixed sites and conducting field campaigns on both land and ships around the world for over two decades.

systems over considerable ranges (60–150 km) as a result of their ability to penetrate precipitating systems while experiencing little attenuation.

Millimeter-wavelength radars are more sensitive to small cloud droplets (Kollias et al. 2007; Lhermitte 1987) because the radar backscatter cross section of water drops increases as the wavelength decreases from centimeter (S, C, X band) to millimeter (Ka, W band) wavelengths. High-power transmitters available at cm-wavelength radars can offset the Rayleigh scattering gains of mm-wavelength radar; however, at low radar reflectivity, the Bragg return dominates the radar signal at cm-wavelength radar. However, attenuation is also larger at the smaller wavelengths, so much so that Ka- and W-band signals suffer severe attenuation that introduces uncertainties in observed cloud properties.

The requirement of improved quantitative retrievals of cloud and precipitation microphysics and dynamics dictated the use of methodologies to overcome one of the most fundamental limitations of radar observations: the fact that the radar return power (i.e., reflectivity factor) is strongly weighted by the larger particles and the relationship between radar reflectivity factor and particle size gets much more complex for frozen particles. This makes the retrieval of lower moments of the particle size distribution (PSD), such as total number particle concentration and water content, which are used to parameterize process rates in high-resolution models, subject to large uncertainties. The methodologies adopted by ARM for this purpose included deployment of dual- and triple-frequency radars to exploit hydrometeor differential absorption and scattering signals, polarimetry, and spectral measurements. These new radar observables were introduced in parallel with significant improvements in radar architecture and technology.

The most recent chapter of ARM radar advancements began in 2011 when the first generation of millimeter-wavelength cloud radars (MMCRs; Moran et al. 1998) were replaced by the Ka-band ARM zenith radars (KAZRs; Fig. 2a). The KAZRs incorporated antennas with improved sidelobe performance, dual-receiver capability to accommodate the simultaneous transmission of a short pulse and a longer pulse with pulse compression to allow faster cycling between modes, and fully digital receiver technology to enable 100% data efficiency. In parallel, a motion-stabilized W-band ARM cloud radar (WACR) was developed

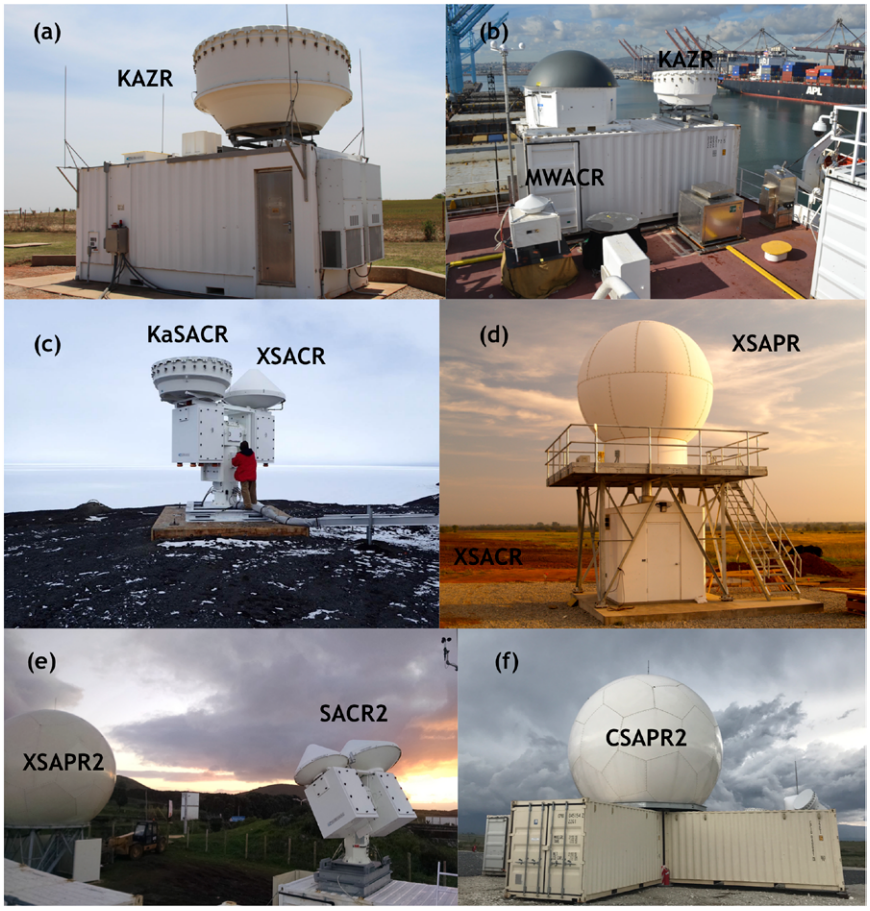

Fig. 2. Examples of ARM radar network radars: (a) the KAZR at the Southern Great Plains, Oklahoma, site; (b) the KAZR and the M-WACR during the Marine ARM GPCI Investigation of Clouds (MAGIC) deployment on board the container ship *Horizon Spirit* out of Long Beach, California; (c) an SACR during the ARM West Antarctic Radiation Experiment (AWARE) deployment in McMurdo Station, Antarctica; (d) one of the three XSAPR's at the Southern Great Plains, Oklahoma, site; (e) the XSAPR2 and the SACR2 at the Eastern North Atlantic (ENA) fixed observatory; and (f) C-SAPR2 during the Cloud, Aerosol, and Complex Terrain Interactions (CACTI) deployment in Argentina.

for ship-based deployments (Fig. 2b). In addition, six scanning ARM cloud radars (SACR's; Kollias et al. 2014a,b) were developed followed by two second-generation SACRs several years later. Each SACR system was composed of a dual-frequency radar system (3 Ka-/W-band SACRs and 3 Ka-/X-band SACRs) with a 0.3° beamwidth capable of exploiting differential absorption and scattering signals to improve quantitative microphysical retrievals (Fig. 2c). The first-generation SACRs offered single polarization on transmit and dual-polarization on receive; however, the two recently fielded second-generation Ka-/W-band SACRs offer full dual-polarization capability to expand information content on nonspherical hydrometeors (Fig. 2e; Lamer et al. 2019).

To expand DOE process research into precipitating clouds and deeper convection, ARM undertook a considerable investment in centimeter-wavelength radars. Four 1.0°-beamwidth X-band scanning ARM precipitation radars (XSAPRs; Fig. 2d) were deployed, one to the ARM North Slope of Alaska (NSA) observatory and three in a network configuration at the ARM Southern Great Plains (SGP) observatory (Fig. 3; North et al. 2017; Oue et al. 2019). A 1.0°-beamwidth C-band scanning ARM precipitation radar (CSAPR) was also deployed to the ARM SGP observatory to provide a comprehensive, heterogeneous, distributed radar network (Borque et al. 2014; North et al. 2017). By 2017, ARM had fielded two unique, second generation SAPRs. The first was a 0.5°-beamwidth, dual-polarization XSAPR (Fig. 2e) deployed to the Eastern North Atlantic (ENA) observatory for the study of shallow, oceanic cloud systems (Lamer et al. 2019). A transportable, 1.0°-beamwidth dual-polarization second-generation CSAPR (Fig. 2f) was also added to the network to improve coverage of deeper convective clouds during ARM Mobile Facility (AMF; Miller et al. 2016) deployments. Additional information regarding core technical capabilities of ARM radar systems and related scientific opportunities, which will be the focus of the following sections, are listed in Table 1.

It has always been ARM's strategy to go beyond short field deployments and collect long-term continuous observations so a range of conditions is observed—enabling a more comprehensive analysis of a given phenomenon (Fig. 1). In addition, ARM does conduct shorter-length field campaigns usually in conjunction with its fixed-location or mobile facility stations to augment those long-term measurements. These intensive periods may include aerial measurements and/or guest instruments. Radars fall somewhere between long-term capabilities and intensive periods. These instruments are highly configurable and can be used in many ways to best sample the cloud and precipitation systems at a particular location while accounting for other logistical constraints. For instance, the Southern Great Plains site hosts a KAZR, a Ka-/W-band SACR, three XSAPRs, a dual-polarization XSAPR, and a CSAPR (Fig. 3). This group of radars constitutes the first continuously operating heterogeneous, distributed radar network intended to sample from shallow cumulus to severe convective cells. Examples of shallow and deep convection observations from the SGP radar network are provided in Borque et al. (2014) and North et al. (2017). In contrast, the North Slope of Alaska site radars have pioneered application of multifrequency, dual-polarization, and spectral radar observations to mixed-phase cloud studies, while more recent Eastern North Atlantic site radars include the narrowest-beamwidth XSAPR2 to facilitate marine low-altitude cloud and drizzle research. The following section describes the ARM efforts to develop a sustainable operational paradigm for these instruments: how new methods to deal with calibration and maintenance of so many different systems had to be developed, how to manage a large diverse set of radars and finally thinking outside the box in terms of how the user can be linked with data of interest.

ARM radar measurement characterization

With deployment of its new radars starting in 2009, a top priority of the radar engineering team was the development of tools to track radar performance, data calibration, and overall data quality. In addition, there was also an awareness of the need to advance the characterization

Table 1. Radar capabilities, notable improvements, and possible scientific applications.

Radar name	Notable improvements/capability	Examples of science application
	Profiling millimeter-wavelength radars	
Ka-band ARM zenith radar (KAZR)	High dynamic range receiver	Hydrometeor location
	Simultaneous transmit and receive of short and chirp[a] pulses	Air motion
		Hydrometeor phase classification
		Hydrometeor fall speed
		Drizzle location
Second-generation KAZR (KAZR2)	KAZR capabilities +[b] transmit pulse amplitude tampering	KAZR applications
	Scanning millimeter-wavelength radars	
Ka- and X-band scanning ARM cloud radar (Ka-X SACR)	Scanning	Cloud mapping over 20 km domain
Ka- and W-band scanning ARM cloud radar (Ka-W SACR)	Common pedestal	Cloud life cycle
	Beam matching	
	Dual frequency	
	Spectra collection	
Second-generation Ka-W SACR (Ka-W SACR2)	SACR capabilities	SACR applications + liquid water content retrieval
	+ Dual polarization	
	+ Optimized beam matching	
	+ Frequency hopping[c]	
	+ Staggered PRT[c]	
	Scanning centimeter-wavelength radars	
X-band scanning ARM precipitation radar (XSAPR)	Dual polarization	Hydrometeor type classification
		Horizontal and vertical velocity
Second-generation XSAPR (XSAPR2)	XSAPR capabilities	XSAPR applications
	+ Narrower antenna beamwidth	+ Surface precipitation mapping
	+ Enhanced sensitivity	over 60 km domain
CSAPR	Dual polarization	Hydrometeor type classification and winds
Second-generation CSAPR (CSAPR2)	CSAPR capabilities + transportable	CSAPR applications

[a] Nonlinear frequency modulation.

[b] + denotes additional capabilities resulting from the second-generation upgrade.

[c] No spectra collection.

of existing (archived) radar datasets. One shared outcome of these efforts was identifying the locations and periods of well-conditioned radar performance (including data epochs, e.g., "ARM Data Discovery Center and the identification of data epochs" section) and advertising those data to the scientific community.

Measurement collection and characterization: The radar operation plan. The operation and characterization of the ARM radars is a strenuous challenge, made distinctive by the following factors: (i) the ARM radar network has more than 20 radars spread around the world (Fig. 2); (ii) the radars in the network were developed by different manufacturers and operate at different frequencies (Table 1); (iii) the radars are operated in remote areas, often with limited connectivity and poor power; (iv) the radars operate under scheduling demands associated with field campaigns, deployments, and redeployments with the AMFs that constrain

maintenance periods; and (v) the radar engineering and operations team is small relative to the number and different types of radars and deployments that it must support. This low ratio of technical staff to instruments is standard for ARM and is enabled through coordination of on-site technical staff with instrument mentors who manage specific instruments, data processing, and data quality assessment. During the early years of the network, the simultaneous deployment of several one-of-a-kind radar systems in remote locations challenged this operational model for the radar network. In recent years, the ARM radar engineering team has worked with the science community and ARM management to identify the highest priority instruments for the coming year. This annual planning has also involved cycling through entire radar systems (using alternative radars with similar capabilities) and maintenance and service of those that have been requested for immediate redeployment and has resulted in significant improvement in radar performance in terms of radar up time and polarimetric and spectral data quality.

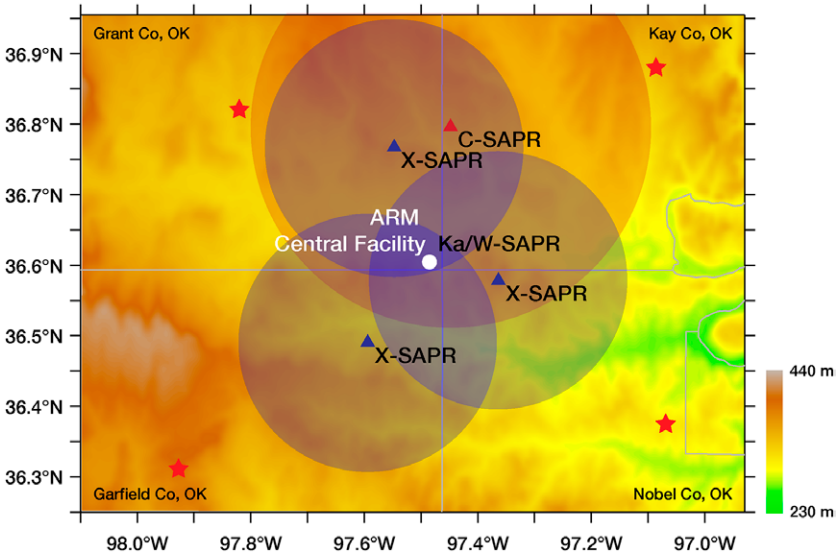

Fig. 3. The heterogeneous, distributed ARM radar network at the SGP. The SGP observatory has installed profiling modules (red stars) at four Extended Facilities to provide measurements in addition to those normally obtained at an Extended Facility site (www.arm.gov/sites/sgp/E). The profiling modules consist of the following instruments: an Atmospheric Emitted Radiance Interferometer (AERI) or Atmospheric Sounder Spectrometer for Infrared Spectral Technology (ASSIST; www.arm.gov/instruments/aeri or www.arm.gov/instruments/assist), a 3-channel microwave radiometer (MWR3C; www.arm.gov/instruments/mwr3c), and a Doppler lidar (DL; www.arm.gov/instruments/dl).

An ongoing strength and challenge of the ARM radars stems from their radar frequency and operational diversity. The different radars each generate their own complex set of diagnostic information. With over 20 radars having different hardware configurations, assimilating all of the diagnostic information necessary for instrument maintenance represents a very time-consuming task. To address this complexity, ARM designed a platform called the Watchdog for ARM Radar Network Operations (WARNO; https://github.com/ARM-DOE/warno). WARNO is a multilevel distributed open source set of software, written in Python, which monitors hundreds of diverse streams of data on each radar and homogenizes them to a common format and within a single framework. Each installation of WARNO has an extensible and configurable plugin architecture that allows for quick assessment of radar health.

Calibration of each radar is one of the most critical and necessary parts of radar operations where the data are used for both qualitative and quantitative applications in radar meteorology (Atlas 2002; Frech et al. 2017; Moisseev et al. 2002). ARM radars contain built-in test equipment that is used to continuously monitor the stability of the radar and the performance of its subsystems, but achieving an absolute calibration requires additional measures. The ARM radar network includes both profiling and scanning millimeter- and centimeter-wavelength radars, thus, achieving absolute calibration requires a number of different strategies. A detailed description of such calibration methods are provided in Bharadwaj et al. (2013) and Chandrasekar et al. (2015). ARM radar operations employ two unique strategies for calibration of remotely deployed systems: 1) field deployable millimeter-wave calibration/measurement equipment, and 2) the use of corner reflectors for calibration.

Millimeter-wave test equipment, such as signal generators, is expensive, bulky, and not designed to be used in the field. Therefore, ARM radar operations developed a portable millimeter-wave calibration kit that can be used by field engineers to calibrate its radars. Figure 4a shows the calibration kit used to make field measurements on the KaSACR. The calibration kit consists of a custom field deployable signal generator for Ka band and W band, precision attenuators, waveguide couplers and calibrated handheld test equipment with USB interface (Bharadwaj et al. 2013). The field deployable calibration kit provides invaluable measurements for calibration. These have been used effectively several times over the past two years in pilot activities and are now being developed for deployment with each ARM observatory. Figure 4b presents a schematic illustration of a triangular trihedral corner reflector for calibrating a radar, whereas Figs. 4c and 4d shows the impact on calibration of corner reflector measurements. This is the only method available for performing absolute calibration including of the antenna. The corner reflector is used when applicable and feasible. In some cases, the terrain or lack of feasible sites makes it impossible to use a tower with a corner reflector. When available, the corner reflector is used to calibrate the SACR. Subsequently, a statistical comparison between the reported SACR and KAZR radar reflectivities when both pointing vertically, is used to monitor the KAZR calibration.

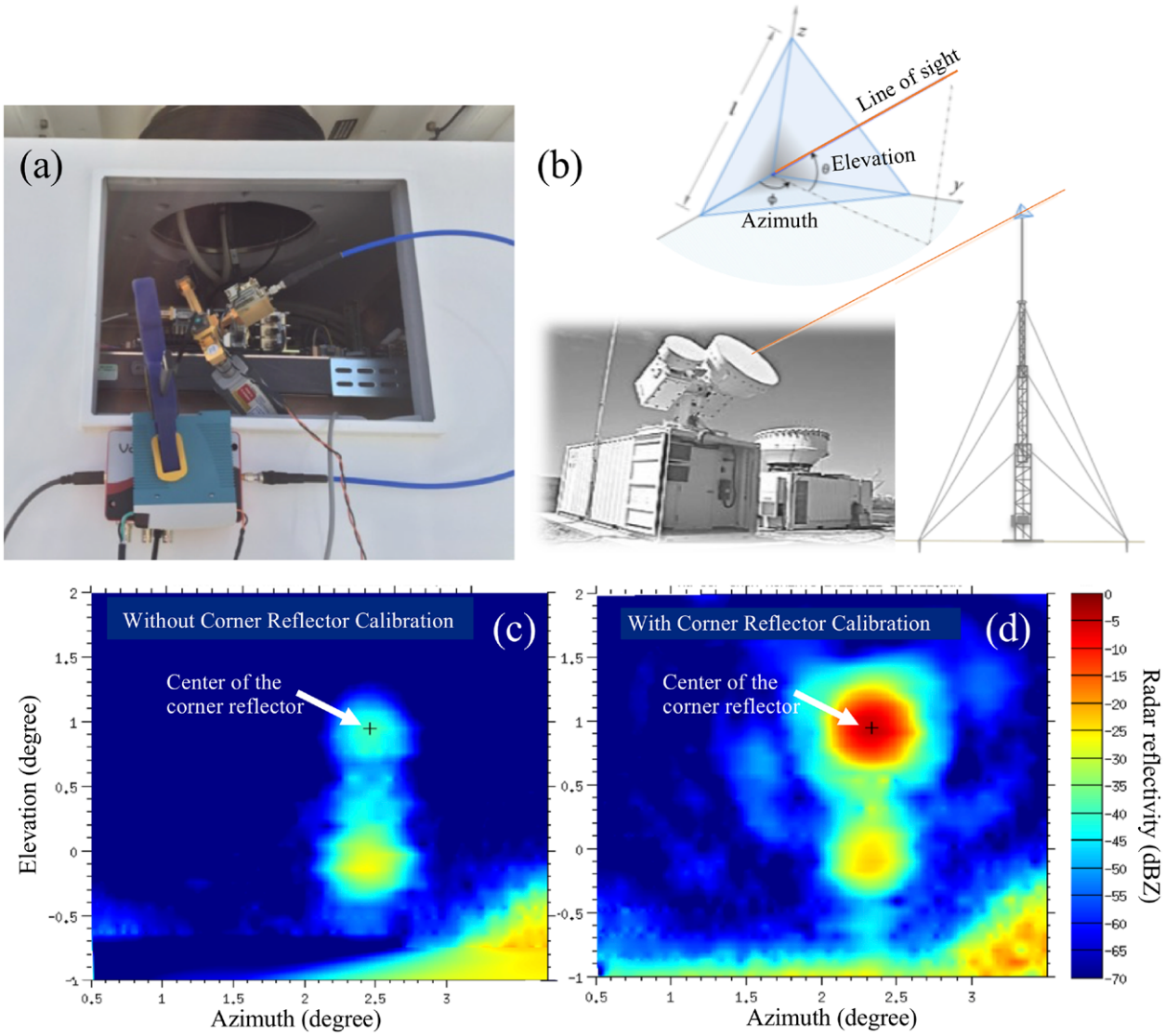

Fig. 4. Calibration setup for the ARM radars: (a) custom kit for calibration of millimeter-wavelength radars in the field; (b) illustration of a triangular trihedral corner reflector for calibration; and calibration of a Ka-SACR with a poorly calibrated antenna (c) without and (d) with supporting corner reflector calibration measurements.

***Historic radar record characterization using* CloudSat.** In addition to ongoing operations and characterization efforts, ARM-supported efforts have also attempted to characterize the longer-term cloud radar profiling record using spaceborne radar observations. Due to their unique stable operating environment and the availability of well-understood natural targets such as the ocean surface (Li et al. 2005), spaceborne radars such as NASA's *CloudSat* Cloud Profiling Radar (CPR) are well calibrated over their entire data records (Tanelli et al. 2008). Protat et al. (2011) first demonstrated that the CPR can be used to characterize the calibration of profiling millimeter-wavelength radars. This methodology was adapted for the calibration of almost the entire ARM cloud profiling radar record during the period from 2007 to 2017 (Kollias et al. 2019). In total, ARM cloud profiling radar observations from 18 different fixed and mobile sites, totaling over 43 years of observations were calibrated. This effort indicated considerable differences between the CPR and the different generations of ARM profiling cloud radars evaluated (MMCR, KAZR, KAZR2). In most cases the differences exceeded the uncertainty of the technique (1–2 dB). ARM is looking into ways to incorporate the reported calibration offsets of its radars against CPR in its radar data records. The Earth Clouds, Aerosol and Radiation Explorer (EarthCARE; Illingworth et al. 2015; Kollias et al. 2018, 2014c) scheduled to launch in 2022 will provide similar to *CloudSat* spaceborne radar measurements to evaluate the ARM radar network calibration in the future.

ARM Data Discovery Center and the identification of data epochs. ARM has collected continuous observations across its network of observatories for over 25 years. This network currently includes over 400 instruments and thousands of data streams. The diversity and volume (dominated by the radars) of ARM data represent a unique wealth of information, but they also pose a challenge in connecting potential science users of ARM data to the data streams and specific measurement periods that would be most beneficial to their research. To facilitate the discovery of high-quality, scientifically relevant time periods, ARM is now working with users to identify and characterize data epochs. Data epochs are time periods, in specific data streams with known calibration, of well-characterized data quality and with quantified uncertainties. ARM staff and data users have identified a number of scientifically interesting time periods to help grow this type of dataset organization. A simple example of a scientifically interesting case would be periods when cold air outbreaks occur during the Cold-Air Outbreaks in the Marine Boundary Layer Experiment (COMBLE). A metadata flag that will identify such periods will allow the data to be selected as part of the ordering process.

Dissemination of data epochs requires a new way of thinking about packaging data for users. Multiple data streams may have overlapping data epochs, leading to the desire to merge datasets to common temporal resolutions and provide data quality reports integrated with standard quality control information currently supplied in data files. In addition, standardization of calibration, uncertainty, and data quality metadata is critical to straightforward merging of multiple data streams and their application to retrieval algorithms or model evaluation projects. Modifications to the ARM data discovery tool will also facilitate users to search and discover epochs along with standard ARM datasets. Currently, ARM packages and disseminates most single instrument data streams as daily files. Changes to this paradigm may help facilitate more flexible data ordering and packaging choices for users.

Science applications

Deployment of the new radars has allowed improved measurement capabilities and new opportunities for the study of cloud and precipitation processes. New capabilities include retrieval of hydrometeor spatial distributions, rainfall rates, and rainfall accumulations over a large domain. Another key emphasis has been on measurements that better constrain column microphysical and kinematical retrievals (e.g., vertical velocity) in clouds and precipitation.

Column capabilities. Interpretation of the radar Doppler moments from a profiling cloud radar is challenging. The radar reflectivity factor is dominated by large drops and the mean Doppler velocity and spectrum width contain both microphysical and dynamical contributions that are difficult to separate (Kollias et al. 2011). Under certain assumptions (e.g., the absence of drizzle drops), the radar Doppler velocity can be used to extract information about cloud dynamics (e.g., Ghate et al. 2011; Kollias and Albrecht 2010; Lamer et al. 2015). In 2006 the ARM profiling radars were upgraded to record full radar Doppler spectra at high temporal and spectral resolution (Kollias et al. 2007). Recording full radar Doppler spectra offers several benefits, enabling removal of radar artifacts (Kollias et al. 2005), identifying and filtering out radar returns contaminated by insects (Luke et al. 2008), detecting supercooled liquid in mixed-phase clouds (Luke et al. 2010; Shupe et al. 2008), and exploiting "Mie notches" (i.e., reductions in the backscattered power with increasing particle size) generated by drops larger than the radar wavelength to retrieve both raindrop size distributions and air motions simultaneously (Kollias et al. 2002, 1999). The upgrade to the KAZR allowed substantially improved radar Doppler spectra quality and led to the development of additional spectral-based microphysical and dynamical retrievals. Improved spectral velocity resolution resulted in improved detection of supercooled liquid spectral peaks near 0 m s^{-1} velocity in mixed-phase clouds (Giangrande et al. 2016; Kalesse et al. 2016; Oue et al. 2018) and the detection of drizzle onset in warm clouds (Luke and Kollias 2013).

In addition, the KAZR has a fully digital receiver with 100% data efficiency, higher dynamic range, reduced signal artifacts, and lower pulse compression sidelobes compared to the MMCR. These KAZR advantages, combined with measurements from the ARM micropulse lidar (MPL) and microwave radiometer (MWR), have significantly improved our ability to detect

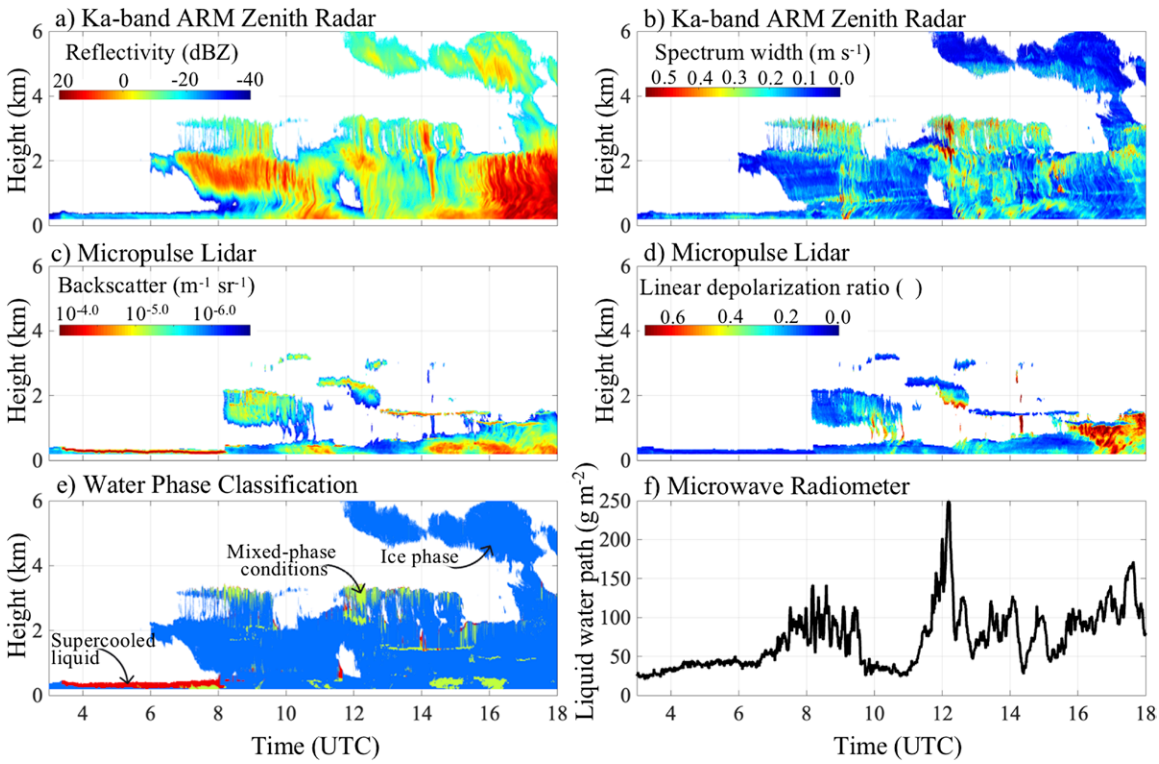

Fig. 5. Measurements collected on 10 Mar 2013, at the North Slope of Alaska observatory of (a) Ka-band ARM zenith radar calibrated copolar reflectivity, (b) Ka-band ARM zenith radar copolar spectrum width, (c) micropulse lidar range-corrected calibrated lidar backscattered power, (d) micropulse lidar linear depolarization ratio, (e) water phase classification [red: liquid water, blue: ice crystals, and green: mixed-phase; retrieval details given in Lamer et al. (2018)], and (f) microwave radiometer retrieved liquid water path [retrieval details given in Turner et al. (2007)].

hydrometeor phase in ice and mixed-phase clouds (Fig. 5). Under mixed-phase conditions, both radars and lidars exploit the fact that nonspherical ice particles and spherical liquid droplets respond differently to polarized light to distinguish between the two water phases (Hogan and O'Connor 2004). Regions such as the one presented in Fig. 5 from 0300 to 0800 UTC of high lidar copolar backscatter (Fig. 5c) and low lidar linear depolarization ratio (Fig. 5d) are indicative of the presence of numerous spherical drops. This inference is also consistent with low copolar radar reflectivity (Fig. 5a), hence all three observables indicating the presence of liquid water (Fig. 5e, red region). Regions such as the one presented in Fig. 5 from 1400 to 1700 UTC with high radar reflectivity (Fig. 5a), high lidar backscatter (Fig. 5c), and low lidar depolarization are indicative of the presence of large particles, such as snow, dominating the radar return and small spherical particles, such as liquid cloud drops, dominating the lidar return; together, these observables suggest the presence of mixtures of liquid and ice particles (Fig. 5e, green region).

Unfortunately, because of strong attenuation of visible to near-infrared lidar signals by cloud drops, the radar-lidar synergy does not generally extend beyond a first cloud layer. For multilayered systems, such as the one presented in Fig. 5 from 1100 to 1300 UTC, radar Doppler spectral width, which typically increases with the number of cloud and precipitation species coexisting in the sample volume and with turbulence, has been put forward as an alternative way to determine water phase (Lamer et al. 2018; Shupe 2007). Additional information from passive microwave radiometer radiance measurements is also routinely used to confirm the presence and quantify the amount of liquid water contained in an atmospheric column (Fig. 5f). Such widely available observations have been used to train Doppler spectra-based algorithms aiming to detect supercooled liquid and isolate its contribution to the radar observables (Luke et al. 2010; Rambukkange et al. 2011; Shupe et al. 2004; Yu et al. 2014). These techniques are not universal, as they tend to be limited to conditions where the observed bimodal Doppler spectral peaks are clearly separated in the radar Doppler spectra by radar noise only containing spectral velocity bins.

Quantitative microphysical retrievals have also benefitted from the deployment of multifrequency radars. Deployment of the Ka- and W-band SACR2 radar pair with collocated beam widths, range resolution volumes, and time samples offers the opportunity to exploit differential wavelength attenuation. On average, as part of their sampling strategy, the SACR's spend 25%–50% of the time pointing vertically. In this configuration, the 1 s integration time improves their sensitivity and reduces the uncertainty in the radar observables. Thus, the majority of the studies conducted using dual-wavelength radar measurements use profiling SACR observations. The difference in radar reflectivity (in dB) measured at two wavelengths, referred to as the dual-wavelength ratio (DWR) can be used to infer information about hydrometeor mass content and size. If the two radar reflectivity measurements are from particles in the small to the wavelength scattering regime, DWR provides a path to retrieving liquid water content (LWC) in clouds without a priori knowledge of the shape of the liquid water content profile or the droplet size distribution. This approach has the additional advantage of not requiring absolutely calibrated radar reflectivity observations (e.g., Eccles and Mueller 1971; Hogan et al. 2005; Huang et al. 2009; Li and Moisseev 2019; Martner 1993; Matrosov et al. 2019; Vivekanandan et al. 1999; Zhu et al. 2019) An example of DWR-based LWC in liquid clouds is discussed in the next section and details of the application of the techniques on the SACR2 are discussed in Zhu et al. (2019). In very shallow clouds (less than 200 m thick), techniques that combine radar and radiometer measurements are also preferred (Küchler et al. 2018). Another promising DWR technique uses radars like the Ka-W SACR that collects dual-frequency Doppler spectra and, in combination with "Mie notches" techniques, the Ka-W SACR produces measurements that support retrievals of both air motion and rain drop size distributions (e.g., Tridon and Battaglia 2015; Tridon et al. 2013). Overall, the column

Fingerprinting microphysical processes in mixed-phase clouds

Arctic ice- and mixed-phase clouds are challenging to study using profiling, single-frequency radar observations due to large natural variability in their ice particle properties and the presence of supercooled liquid (Shupe et al. 2008). The availability of collocated, multisensor profiling observations at the ARM NSA observatory makes it possible to untangle some of the complex microphysics in play within the mixed-phase clouds there. For example, Ka/W-SACR polarimetric variables capture ice/snow particle shape properties and complement the Doppler spectra information on coexisting liquid and ice particles, as well as air motion (Kalesse et al. 2016). Polarimetric variables collected by scanning radars, however, are not readily compared to zenith Doppler spectra because the majority of polarimetric radar observables contain the most information when they are collected at lower elevation angle scans and do not overlap with vertically collected profiles. The generation of quasi-vertical profiles that involves averaging the polarimetric radar observables over azimuth angle at each range helps to connect scanning and zenith observations (Fig. SB1a; Oue et al. 2018; Ryzhkov et al. 2016). Simultaneous utilization of multiple radar wavelengths further exploits frequency-dependent backscattering properties of cloud and precipitation particles, providing additional information on their species and sizes (Kneifel et al. 2011, 2015; Leinonen and Moisseev 2015; Oue et al. 2015; Yoshida et al. 2006).

For example, different hydrometeor particles produce distinct velocity modes in Doppler spectra, as seen in Fig. SB1b where the modes in the Doppler spectra with height depend on particle masses, sizes, and number concentrations. Weaker peaks in the Doppler spectra near 0 m s^{-1} Doppler velocity are attributed to liquid cloud droplets, whereas stronger peaks having a persistent and significant downward Doppler velocity over time represent falling ice particles. Of the falling ice particles, those with faster downward velocities are typically compact, higher-density particles. Larger dual-wavelength ratios (Fig. SB1c) indicate large snow particles. Dual-polarization quantities such as differential reflectivity (ZDR) help to infer particle size and aspect ratio, whereas the specific differential phase (KDP) informs us about ice water content and aspect ratio (Fig. SB1d). Only by combining the different observables from these different sources are we able to identify processes such as ice particle aggregation, riming growth, and vapor depositional growth (Fig. SB1e).

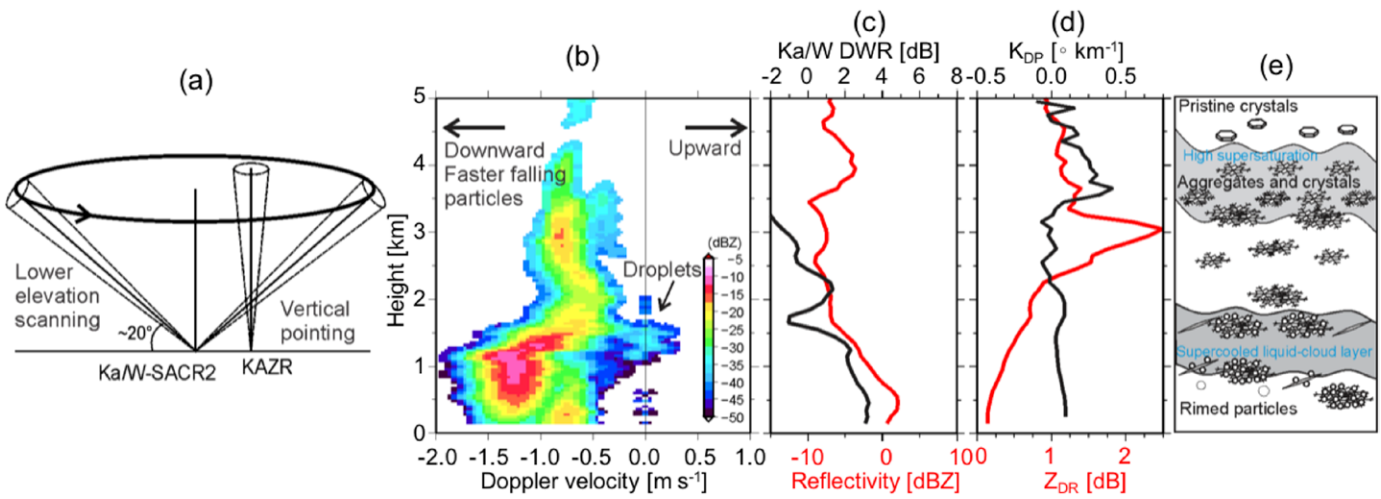

Fig. SB1. (a) A schematic diagram of joint observations using zenith pointing radar (KAZR2) and scanning radar (Ka/W SACR2) quasi-vertical profiling (QVP) techniques. (b) Doppler spectrum diagram from the KAZR2 at the ARM Mobile Facility in Oliktok Point, Alaska. QVPs of (c) Ka-band radar reflectivity (red line) and DWR of Ka vs W bands (black line), and (d) Ka-band Z_{DR} (red line) and Ka-band K_{DP} from the Ka/W-SACR2 (black line) from the ARM Mobile Facility. (e) Schematic diagram of identified hydrometeor particles and estimated ice microphysical processes.

measurement capabilities of the ARM radar network have improved substantially with the addition of multiwavelength, spectral, and polarimetric information. An example of use of profiling and scanning SACR2 observations in arctic mixed-phase when the hydrometeor sizes are comparable to the radar wavelengths is discussed in the "Fingerprinting microphysical processes in mixed-phase clouds" sidebar.

Domain capabilities. Vertically pointing sensors profile clouds and precipitation as they develop or are advected overhead by the horizontal wind. When cloud advection speed is more rapid than cloud evolution, such observations are interpretable as representing the horizontal structure of clouds (e.g., Lamer et al. 2015); otherwise, distinguishing cloud horizontal structure from cloud

evolution remains challenging. At the ENA observatory, ARM operates a narrow-beamwidth (0.5°) XSAPR2 capable of mapping the mesoscale cloud and precipitation organization over an effective range of 40–60 km (Lamer et al. 2019). The XSAPR2 has sufficient sensitivity (–21 dB*Z* at 20 km, no integration; Lamer et al. 2019) and provides for the first-time direct measurements of the horizontal structure of precipitation at the ENA observatory (Fig. 6a). The XSAPR2 observations are used to

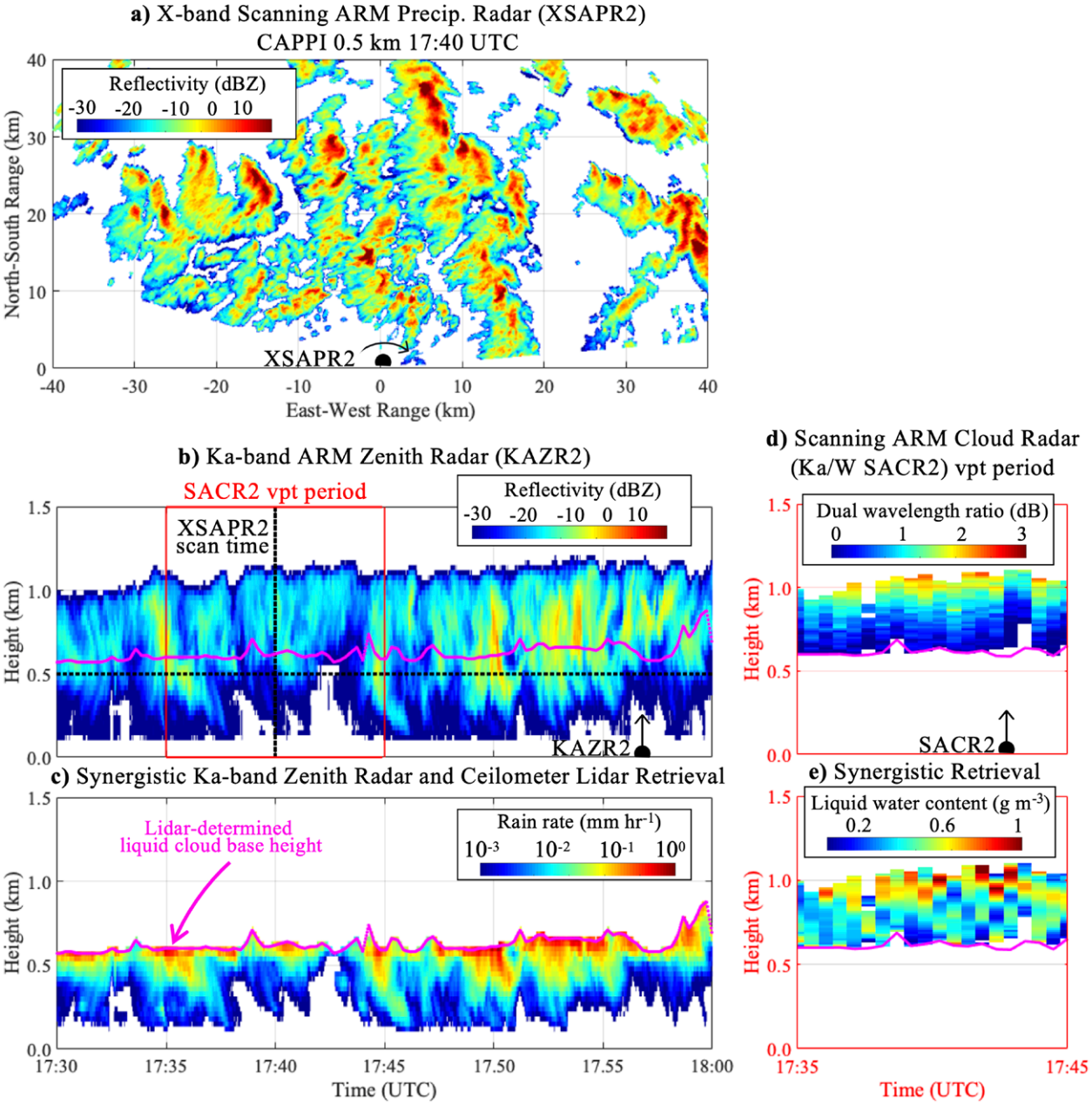

Fig. 6. Measurements collected on 9 Feb 2018, at the Eastern North Atlantic observatory of (a) X-band scanning ARM precipitation radar calibrated copolar reflectivity collected at 1740 UTC in plan position indicator (PPI) mode presented as a 0.5 km constant-altitude PPI (CAPPI) constructed from a number of different elevation PPI's, and (b) Ka-band ARM zenith radar calibrated copolar reflectivity. The vertical dashed line indicates the approximate time when the corresponding XSAPR2 CAPPI data were collected (takes a total of 3 min to complete all the PPI's needed to generate the CAPPI data) and the horizontal dashed line indicates when average height of the CAPPI, and (c) rain-rate retrievals performed by combining the Ka-band zenith radar copolar reflectivity illustrated in (b) and ceilometer lidar backscatter measurements (not illustrated) following O'Connor et al. (2005). For the period enclosed in the red box in (b), (d) Ka/W scanning ARM cloud radar dual-wavelength ratio and (e) cloud liquid water content retrieval performed from the Ka/W-band dual-wavelength ratio illustrated in (d) following Zhu et al. (2019). The lidar-determined lowest-altitude liquid cloud-base heights are also illustrated in (b)–(e).

monitor and study the temporal three-dimensional evolution of shallow precipitating cells that may never advect over vertically pointing sensors, making the XSAPR2 observations especially useful in studies of horizontally inhomogeneous domains (e.g., Fig. 6a). The ENA XSAPR2 measurements are often difficult to reconcile with corresponding profiling observations (Figs. 6b,c). A combination of vertically pointing and scanning radar observations remains as today's best option for characterizing weak and/or vertically inhomogeneous meteorological events (Lamer et al. 2019). Similarly, under conditions where cloud and precipitation particles are mostly spherical, millimeter-wavelength radar reflectivity (Fig. 6b) and near-infrared lidar backscatter cross sections have been combined to retrieve microphysical properties, such as rain rate (Fig. 6c; O'Connor et al. 2005). For the period enclosed in the red box of Fig. 6b, the Ka/W-SACR2 was vertically pointing and the DWR radar measurements are shown in Fig. 6d. The corresponding cloud liquid water content retrievals performed from the Ka/W-band dual-wavelength ratio following (Zhu et al. 2019) are shown in Fig. 6e. In a nutshell, Fig. 6 illustrates the ability of the ENA radars to capture both mesoscale cloud and drizzle organization and retrieve LWC profiles above and below the cloud-base height.

Borque et al. (2014) provided evidence for the potential of scanning cloud radars like the KaSACR to document the life cycle of shallow clouds when configured to repeatedly and rapidly revisit the same observation volume. On the other hand, centimeter-wavelength radars are more suitable for studying convective cloud life cycles owing to attenuation in rain. For instance, ARM's new dual-polarimetric CSAPR, a part of the ARM Mobile Facility 1 (AMF1), was specifically deployed for the Cloud, Aerosol, and Complex Terrain Interactions (CACTI) field campaign (October 2018–May 2019) in the Argentinean foothills outside Villa Yacanto. In this region, storms regularly form over the Sierras de Cordoba before moving east over the plains, providing a natural laboratory to study cloud life cycle and the opportunity to routinely observe some of the largest storms on Earth (Fig. 7). During the CACTI field campaign, the CSAPR routinely monitored the evolution of storms forming over the mountains before moving east over the plains using a sequence of plan position indicator (PPI) and hemispherical sky range–height indicator (HSRHI) scans. An example of HSRHI scans is shown in Figs. 7a and 7b. HSRHI scans are a standard scan strategy of the CSAPR2 and demonstrate the importance of both sampling a large domain and routinely documenting the column sampled by the vast majority of ARM sensors that point vertically. The aforementioned scan strategy allowed documentation of the vertical structure of these storms while they advected over the ARM observatory. The CSAPR is ARM's latest fully polarimetric radar and its polarimetric observables are designated to investigate the melting layer (Giangrande et al. 2008), differentiate hydrometeor types (Dolan et al. 2013), estimate drop size distribution parameters (Gorgucci et al. 2002), and estimate rain rates (Giangrande et al. 2014). An example of CSAPR2 differential reflectivity (Z_{DR}, in colors) and specific differential phase (K_{DP}, in contours) from the same supercell system shown in Figs. 7a and 7b, but at an earlier time (farther west) in order to improve the polarimetric measurements shown in Figs. 7c and 7d. The Z_{DR} is a measure of the reflectivity-weighted mean axis ratio of the precipitation particle distribution (Hubbert et al. 2018). The high positive Z_{DR} values in the lowest 2–3 km indicate the presence of large oblate raindrops and coincide with high positive K_{DP} values that indicate the presence of large liquid water content. The area of negative K_{DP} values between 6 and 10 km height indicate a zone of ice crystals aligned vertically by an electric field (Hubbert et al. 2018).

Perhaps the most fundamental property of a thunderstorm is its vertical air motion. The ability to improve severe thunderstorm forecasts in numerical weather prediction models is tied to an understanding of these air motions. Unfortunately, updraft and downdraft measurements are elusive for convective cloud studies, with few direct or remote methods to identify and investigate them (e.g., Byers and Battan 1949; LeMone and Zipser 1980). One motivation for ARM's recent upgrade to its SGP facility was to develop a Doppler radar network suitable to the challenges of kinematic retrievals in deeper convective clouds (Fig. 3). An example of

horizontal and vertical wind fields following well-established methods (North et al. 2017) is shown in "The search for *W*: Vertical air motion in deep convection" sidebar. In addition to establishing the radar facility at the SGP, considerable effort was invested in assessing the uncertainty in the vertical air motion retrievals. The comprehensive analysis by Oue et al. (2019) highlighted several shortcomings of the vertical wind retrievals at heights above 6 km using the ARM SGP network. The findings by Oue et al. (2019) resulted to a recent reconfiguration of the radar sampling strategies with more coverage of the higher elevations and will influence future ARM investments in radar systems for the estimation of the vertical air motion in deep convective clouds.

Applying radar observations to model evaluation. Besides contributing to improving our fundamental understanding of clouds and precipitation, observations collected by radar

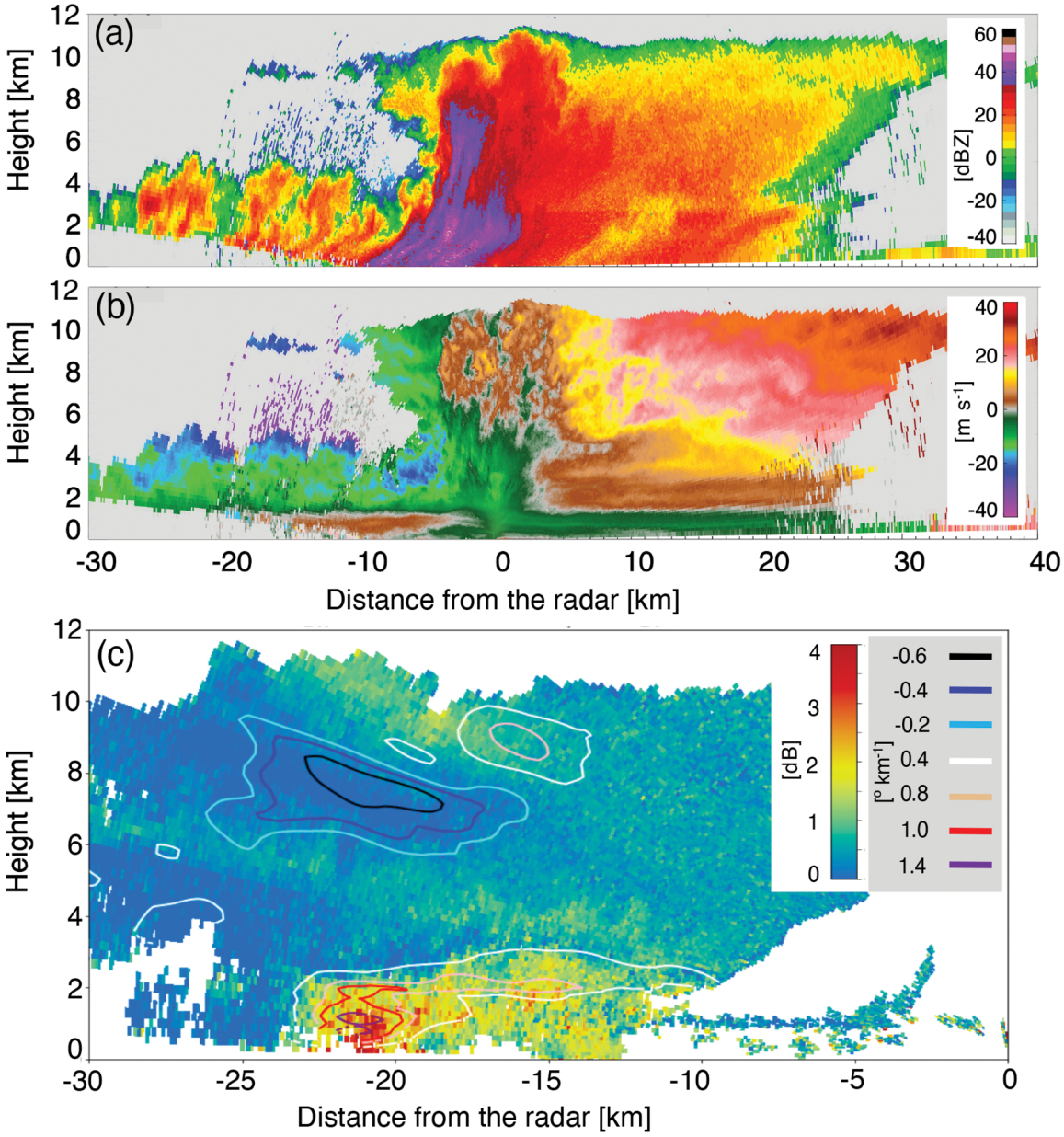

Fig. 7. Vertical cross sections of (a) radar reflectivity and (b) radial Doppler velocity from a hemispherical sky range–height indicator (HSRHI), (c) CSAPR2 differential reflectivity (Z_{DR}, in colors) and specific differential phase (K_{DP}, in contours) from the same supercell system shown in (a) and (b), but at an earlier time (farther west) in order to improve the polarimetric measurements. The observations were collected on 27 Nov 2018.

The Search for *W*: Vertical air motion in deep convection

The need for detailed and long-term observations of deep convection vertical velocities motivated ARM's upgrades to its SGP facility. Since the early work of Lhermitte and Miller (1970), the use of multi-Doppler radar wind retrieval techniques has been widely used to estimate the vertical air motion in convective clouds (Bousquet and Chong 1998; Chong and Testud 1996; Gao et al. 1999; Potvin et al. 2012; Protat and Zawadzki 1999). The SGP facility combines four scanning weather Doppler radars (North et al. 2017). An example of their use for wind retrievals was during the tornadic supercell event of 23 May 2011 that occurred during the Midlatitude Continental Convective Clouds Experiment (MC3E; Fig. SB2). Mass continuity constraints applied to a three-dimensional mosaic of Doppler velocities constructed from the radar network allowed for retrieval of vertical (Fig. SB2a) and horizontal (Fig. SB2b) velocity at any cross section within the storm (North et al. 2017).

The SPG radar network represents only the first effort for developing a continuously operating facility for wind retrievals in deep convection. Oue et al. (2019) conducted a series of observing system simulation experiments (OSSEs) to investigate potential sources of errors in multi-Doppler radar wind retrievals. The study clearly indicated that the vertical air motion retrievals in the upper part of convective clouds (above 6 km) remain challenging using the SGP radar network. Significant improvements are required in the sampling strategy (higher maximum elevation angle, higher-density elevation angles and faster sampling time). These improvements suggest the use of rapid scan radars and the use of adaptive scan strategies to reduce the sampling time. Nevertheless, statistical composites of deep convective dynamics based on routine ARM operations may elucidate climate model scale connections between convective updrafts, precipitation, and storm life cycle.

ARM initiatives also led to the reconfiguration of its radar wind profilers (RWPs) in 2011 to bolster ARM radar network precipitation capabilities (Tridon et al. 2013). As part of their reconfiguration, the RWPs dedicate most of the sampling time in profiling mode, thus, sampling sufficiently fast (3–6 s) the vertical structure of precipitation at the ARM observatories. These recent changes in capability have sparked new thoughts on thunderstorm intensity, core size, and mixing, and relevant controls in midlatitude and tropical convection (e.g., Fan et al. 2018; Giangrande et al. 2013; Schiro et al. 2018; Schiro and Neelin 2018).

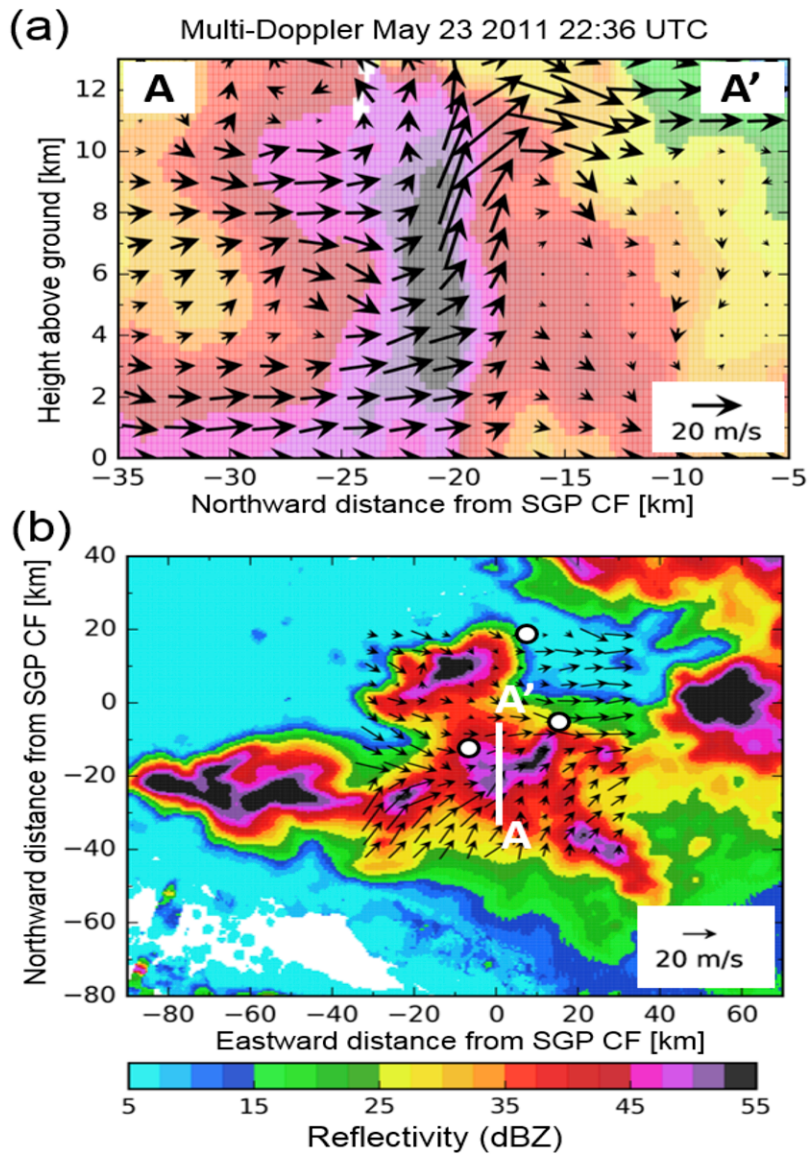

Fig. SB2. (a) Vertical cross section of radar reflectivity (color) and multi-Doppler wind field retrievals (arrows) through the core of an Oklahoma tornadic supercell on 23 May 2011. The vertical cross section corresponds to the A-A' line as drawn in (b). (b) The 3-km above ground level CAPPI of the radar reflectivity and horizontal wind field retrievals. White circles correspond to the locations of the ARM radars used to perform these wind field retrievals.

have been used to evaluate the performance of models of various scales and complexity. For example, multi-Doppler retrieved three-dimensional wind fields have been used to evaluate the intensity of mesoscale convective systems simulated by cloud-resolving models (Fan et al. 2017; Varble et al. 2014), and reflectivity-retrieved rain rates have been used to evaluate precipitation simulated by single column models (Song et al. 2013). In fact, simple radar observations of cloud vertical location as a function of time have been so widely used to evaluate cloud formation in large eddy simulation (e.g., Endo et al. 2015), cloud-resolving models (e.g., Luo et al. 2008; Zeng et al. 2007), numerical weather prediction models (e.g., Ahlgrimm and Forbes 2014), and general circulation models (GCMs; e.g., Song et al. 2014), that ARM has made it a priority to package these measurements in an official value-added product: the Atmospheric Active Remotely Sensed Cloud Locations (ARSCL; Clothiaux et al. 2001). Along with additional information from soundings and microwave radiometer measurements, the ARM "microbase" products (Dunn et al. 2011) provide additional insights on cloud microphysical properties for model evaluation (Zeng et al. 2007). To mitigate issues related to radar detection limitations and signal attenuation that may lead to underestimation of thin cirrus cloud-top heights, ARM also developed a valued-added product that combines observations from millimeter-wavelength radar and near-infrared lidar for an ARM best estimate (ARMBE) of cloud boundary location and cloud fraction for model evaluation (Fu 1996).

Recent work suggests that employing forward simulators allows for a more objective comparison between simulated and observed properties, especially for those that have large retrieval uncertainties. Forward simulators convert modeled geophysical hydrometeor properties to sensor observables, mimicking the sampling geometry and detection limitations unique to each sensor (e.g., Maahn 2015; Zhang et al. 2018). Other more sophisticated simulators are additionally capable of reproducing Doppler moments (e.g., Lamer et al. 2018), polarimetry (e.g., Dolan et al. 2017; Matsui et al. 2019; Oue et al. 2020) and complete Doppler spectra observables (Oue et al. 2020). These forward operators allow us to investigate the relationships between observed parameters both in the observational and in the model world and facilitate a more complete evaluation of modeled microphysical processes, such as ice formation (van Diedenhoven et al. 2009) and drizzle size distributions (Rémillard et al. 2017).

Although case studies to date have provided a wealth of information on model performance, longer-term observations would likely uncover more generalized model issues. Unfortunately, statistically summarizing hydrometeor attributes while not masking compensating biases is not simple because a number of processes, both large-scale and microphysical, affect cloud and precipitation growth, lifetime, and decay. Moreover, it is desirable that such simplified statistical summaries maintain sufficient information to diagnose the cause of identified biases. Recently, Zhang et al. (2018) published an ARM cloud radar simulator for GCM's that can be used to evaluate their performance at the proximity of the ARM sites using long-term ground-based radar reflectivity observations that provide information on the vertical distribution of hydrometeors.

Epilogue

The ARM radar network has evolved significantly from its origins in the mid-1990s when vertically profiling millimeter-wavelength radars were first deployed. Today, the network is a unique observational resource that brings together a broad array of radar technologies to enable the combined analysis of clouds and precipitation. These measurements are further coupled with an array of other ARM instruments that provide information from the background atmospheric state, to properties of clouds, precipitation and aerosols, to the surface energy budget. This network represents a unique community resource on multiple fronts and is continuing to advance. Past and present foci include the following.

Establishing and maintaining operational millimeter-wavelength radars. Since the early days of ARM, profiling millimeter-wavelength radars have been an essential part of its surface-based observatories for cloud research. Until ARM, these relatively new, high-frequency radars were available only in a handful of research institutions and universities (Kollias et al. 2007). ARM undertook the challenging task of supporting the maturation of the technology needed to operate these radars in a continuous manner. It is in concert with ARM efforts that profiling millimeter-wavelength radar technology was matured to the point where it could operate in a continuous manner. Equally important efforts by ARM led to increasing the reliability, improving the functionality, and reducing the cost of these radars, enabling them to be deployed in now tens of locations around the world to facilitate cloud research.

Entering uncharted areas in radar meteorology as necessary. Over the last 10 years, the ARM facility, confronted with the challenge of addressing the need for high-resolution cloud and precipitation observations from the cloud scale to the mesoscale, made the decision to significantly expand its radar network. In so doing, it once again positioned itself in uncharted radar meteorology territory and in many different ways. The bridging of centimeter- and millimeter-wavelength radars from different vendors for holistic observations of clouds and precipitation in an operational setting was new. The learning curve in operations, maintenance, and characterization of these various radars continues to be steep for the ARM radar engineering group, but their operations are becoming more stable and there is progress in radar calibration and quality control. As a result of hardware successes, ARM is now pioneering some of the first systematic studies to conduct multiwavelength, polarimetric, and spectral-based radar studies of cloud systems, including high-latitude mixed-phase clouds and low-altitude shallow boundary layer clouds.

Breaking community barriers. In the course of its endeavors, ARM has brought together engineers and scientists from the weather, climate, and radar communities. The merging of these communities has led to new perspectives and innovative ideas, while the availability of the ARM radar network provides an ideal playground for testing and evaluating different sampling strategies and retrieval techniques. In addition, a much larger, demanding user community encompassing all scales of numerical modeling has become interested in ARM radar measurements. The interests of this broad model-based user community have necessitated the deployment of the ARM radar network from deep convective cloud regions to marine deployments on container ships and research vessels. Making best use of these data has pushed ARM forward in the development of comprehensive radar simulators to ease comparisons of the radar observations with model output. In summary, ARM pioneered the tearing down of traditional, artificial barriers between the cloud and precipitation communities both in observations and modeling and is now several steps closer in developing holistic, surface-based observatories.

Acknowledgments. The work presented here was supported by U.S. Department of Energy (DOE) Atmospheric Radiation Measurement (ARM) facility and the Atmospheric System Research (ASR) program. We would like to acknowledge Bernat Puigdomènech Treserras (McGill University) for contributing Fig. 7 and Rolanda Jundt (PNNL) and William Gustafson (PNNL) for contributing Fig. 3. This paper has been authored by employees of Brookhaven Science Associates, LLC, under Contract DE-SC0012704 with the U.S. Department of Energy (DOE). The publisher by accepting the paper for publication acknowledges that the U.S. government retains a nonexclusive, paid-up, irrevocable, worldwide license to publish or reproduce the published form of this paper, or allow others to do so, for U.S. government purposes.

References

Ackerman, T. P., T. S. Cress, W. R. Ferrell, J. H. Mather, and D. D. Turner, 2016: The programmatic maturation of the ARM program. *The Atmospheric Radiation Measurement (ARM) Program: The First 20 Years*, *Meteor. Monogr.*, No. 57, Amer. Meteor. Soc., https://doi.org/10.1175/AMSMONOGRAPHS-D-15-0054.1.

Ahlgrimm, M., and R. Forbes, 2014: Improving the representation of low clouds and drizzle in the ECMWF model based on ARM observations from the Azores. *Mon. Wea. Rev.*, **142**, 668–685, https://doi.org/10.1175/MWR-d-13-00153.1.

Atlas, D., 2002: Radar calibration: Some simple approaches. *Bull. Amer. Meteor. Soc.*, **83**, 1313–1316, https://doi.org/10.1175/1520-0477-83.9.1313.

Bharadwaj, N., K. Widener, A. Lindenmaier, and V. Venkatesh, 2013: Calibration system for ARM radars. *36th Conf. on Radar Meteorology*, Richland, WA, Amer. Meteor. Soc., P260, https://ams.confex.com/ams/36Radar/webprogram/Paper228622.html.

Borque, P., P. Kollias, and S. Giangrande, 2014: First observations of tracking clouds using scanning ARM cloud radars. *J. Appl. Meteor. Climatol.*, **53**, 2732–2746, https://doi.org/10.1175/JAMC-D-13-0182.1.

Bousquet, O., and M. Chong, 1998: A multiple-Doppler synthesis and continuity adjustment technique (MUSCAT) to recover wind components from Doppler radar measurements. *J. Atmos. Oceanic Technol.*, **15**, 343–359, https://doi.org/10.1175/1520-0426(1998)015<0343:AMDSAC>2.0.CO;2.

Bringi, V. N., and V. Chandrasekar, 2001: *Polarimetric Doppler Weather Radar: Principles and Applications*. Cambridge University Press, 636 pp.

Byers, H. R., and L. J. Battan, 1949: Some effects of vertical wind shear on thunderstorm structure. *Bull. Amer. Meteor. Soc.*, **30**, 168–175, https://doi.org/10.1175/1520-0477-30.5.168.

Chandrasekar, V., L. Baldini, N. Bharadwaj, and P. L. Smith, 2015: Calibration procedures for global precipitation-measurement ground-validation radars. *URSI Radio Sci. Bull.*, **2015**, 45–73, https://doi.org/10.23919/URSIRSB.2015.7909473.

Chong, M., and J. Testud, 1996: Three-dimensional air circulation in a squall line from airborne dual-beam Doppler radar data: A test of coplane methodology software. *J. Atmos. Oceanic Technol.*, **13**, 36–53, https://doi.org/10.1175/1520-0426(1996)013<0036:TDACIA>2.0.CO;2.

Clothiaux, E. E., and Coauthors, 2001: The ARM millimeter wave cloud radars (MMCRs) and the active remote sensing of clouds (ARSCL) value added product (VAP). DOE Tech. Memo. ARM VAP-002.1, 56 pp., www.arm.gov/publications/tech_reports/arm-vap-002-1.pdf.

Dolan, B., S. A. Rutledge, S. Lim V. Chandrasekar, and M. Thurai, 2013: A robust C-band hydrometeor identification algorithm and application to a long-term polarimetric radar dataset. *J. Appl. Meteor. Climatol.*, **52**, 2162–2186, https://doi.org/10.1175/JAMC-D-12-0275.1.

——, ——, J. I. Barnum, T. Matsui, W.-K. Tao, and T. Iguchi, 2017: Investigation of hydrometeor classification uncertainties through the POLARRIS polarimetric radar simulator. *2017 AGU Fall Meeting*, New Orleans, LA, Amer. Geophys. Union, Abstract A34A-05.

Doviak, R. J., and D. S. Zrnić, 1993: *Doppler Radar and Weather Observations*. 2nd ed. Academic Press, 562 pp.

Dunn, M., K. Johnson, and M. Jensen, 2011: The microbase value-added product: A baseline retrieval of cloud microphysical properties. ARM Tech. Rep. DOE/SC-ARM/TR-095, 34 pp., www.arm.gov/publications/tech_reports/doe-sc-arm-tr-095.pdf.

Eccles, P. J., and E. A. Mueller, 1971: X-band attenuation and liquid water content estimation by a dual-wavelength radar. *J. Appl. Meteor.*, **10**, 1252–1259, https://doi.org/10.1175/1520-0450(1971)010<1252:XBAALW>2.0.CO;2.

Ellis, S. M., and J. Vivekanandan, 2011: Liquid water content estimates using simultaneous S and Ka band radar measurements. *Radio Sci.*, **46**, RS2021, https://doi.org/10.1029/2010RS004361.

Endo, S., and Coauthors, 2015: RACORO continental boundary layer cloud investigations: 2. Large-eddy simulations of cumulus clouds and evaluation with in situ and ground-based observations. *J. Geophys. Res. Atmos.*, **120**, 5993–6014, https://doi.org/10.1002/2014JD022525.

Fan, J., and Coauthors, 2017: Cloud-resolving model intercomparison of an MC3E squall line case: Part I—Convective updrafts. *J. Geophys. Res. Atmos.*, **122**, 9351–9378, https://doi.org/10.1002/2017JD026622.

——, and Coauthors, 2018: Substantial convection and precipitation enhancements by ultrafine aerosol particles. *Science*, **359**, 411–418, https://doi.org/10.1126/science.aan8461.

Frech, M., M. Hagen, and T. Mammen, 2017: Monitoring the absolute calibration of a polarimetric weather radar. *J. Atmos. Oceanic Technol.*, **34**, 599–615, https://doi.org/10.1175/JTECH-D-16-0076.1.

Fu, Q., 1996: An accurate parameterization of the solar radiative properties of cirrus clouds for climate models. *J. Climate*, **9**, 2058–2082, https://doi.org/10.1175/1520-0442(1996)009<2058:AAPOTS>2.0.CO;2.

Gao, J., M. Xue, A. Shapiro, and K. K. Droegemeier, 1999: A variational method for the analysis of three-dimensional wind fields from two Doppler radars. *Mon. Wea. Rev.*, **127**, 2128–2142, https://doi.org/10.1175/1520-0493(1999)127<2128:AVMFTA>2.0.CO;2.

Ghate, V. P., M. A. Miller, and L. DiPretore, 2011: Vertical velocity structure of marine boundary layer trade wind cumulus clouds. *J. Geophys. Res.*, **116**, D16206, https://doi.org/10.1029/2010JD015344.

Giangrande, S. E., S. Collis, J. Straka, A. Protat, C. Williams, and S. Krueger, 2013: A summary of convective-core vertical velocity properties using ARM UHF wind profilers in Oklahoma. *J. Appl. Meteor. Climatol.*, **52**, 2278–2295, https://doi.org/10.1175/JAMC-D-12-0185.1.

——, ——, A. K. Theisen, and A. Tokay, 2014: Precipitation estimation from the ARM distributed radar network during the MC3E campaign. *J. Appl. Meteor. Climatol.*, **53**, 2130–2147, https://doi.org/10.1175/JAMC-D-13-0321.1.

——, T. Toto, A. Bansemer, M. R. Kumjian, S. Mishra, and A. V. Ryzhkov, 2016: Insights into riming and aggregation processes as revealed by aircraft, radar, and disdrometer observations for a 27 April 2011 widespread precipitation event. *J. Geophys. Res. Atmos.*, **121**, 5846–5863, https://doi.org/10.1002/2015JD024537.

——, J. M. Krause, and A. V. Ryzhkov, 2008: Automatic designation of the melting layer with a polarimetric prototype of the WSR-88D radar. *J. Appl. Meteor. Climatol.*, **47**, 1354–1364, https://doi.org/10.1175/2007JAMC1634.1.

Gorgucci, E., V. Chandrasekar, V. Bringi, and G. Scarchilli, 2002: Estimation of raindrop size distribution parameters from polarimetric radar measurements. *J. Atmos. Sci.*, **59**, 2373–2384, https://doi.org/10.1175/1520-0469(2002)059<2373:EORSDP>2.0.CO;2.

Haeffelin, M., and Coauthors, 2016: Parallel developments and formal collaboration between European atmospheric profiling observatories and the U.S. ARM research program. *The Atmospheric Radiation Measurement (ARM) Program: The First 20 Years*, *Meteor. Monogr.*, No. 57, Amer. Meteor. Soc., https://doi.org/10.1175/AMSMONOGRAPHS-D-15-0045.1.

Hogan, R. J., and J. W. F. Goddard, 1999: Calibration of the ground-based radars used in CLARE'98. *CLARE'98 Final Workshop*, Noordwijk, Netherlands, ESA, 63–67.

——, and E. O'Connor, 2004: Facilitating cloud radar and lidar algorithms: The Cloudnet Instrument Synergy/Target Categorization product. Cloudnet Doc., 14 pp., www.met.rdg.ac.uk/~swrhgnrj/publications/categorization.pdf.

——, N. Gaussiat, and A. J. Illingworth, 2005: Stratocumulus liquid water content from dual-wavelength radar. *J. Atmos. Oceanic Technol.*, **22**, 1207–1218, https://doi.org/10.1175/JTECH1768.1.

Huang, D., K. Johnson, Y. Liu, and W. Wiscombe, 2009: High resolution retrieval of liquid water vertical distributions using collocated Ka-band and W-band cloud radars. *Geophys. Res. Lett.*, **36**, L24807, https://doi.org/10.1029/2009GL041364.

Hubbert, J. C., J. W. Wilson, T. M. Weckwerth, S. M. Ellis, M. Dixon, and E. Loew, 2018: S-Pol's polarimetric data reveal detailed storm features (and insect behavior). *Bull. Amer. Meteor. Soc.*, **99**, 2045–2060, https://doi.org/10.1175/BAMS-D-17-0317.1.

Illingworth, A. J., and Coauthors, 2007: Cloudnet: Continuous evaluation of cloud profiles in seven operational models using ground-based observations. *Bull.*

Amer. Meteor. Soc., **88**, 883–898, https://doi.org/10.1175/BAMS-88-6-883.
——, and Coauthors, 2015: The EarthCARE satellite: The next step forward in global measurements of clouds, aerosols, precipitation, and radiation. *Bull. Amer. Meteor. Soc.*, **96**, 1311–1332, https://doi.org/10.1175/BAMS-D-12-00227.1.
Kalesse, H., W. Szyrmer, S. Kneifel, P. Kollias, and E. Luke, 2016: Fingerprints of a riming event on cloud radar Doppler spectra: Observations and modeling. *Atmos. Chem. Phys.*, **16**, 2997–3012, https://doi.org/10.5194/acp-16-2997-2016.
Kneifel, S., M. Kulie, and R. Bennartz, 2011: A triple-frequency approach to retrieve microphysical snowfall parameters. *J. Geophys. Res.*, **116**, D11203, https://doi.org/10.1029/2010JD015430.
——, A. Lerber, J. Tiira, D. Moisseev, P. Kollias, and J. Leinonen, 2015: Observed relations between snowfall microphysics and triple-frequency radar measurements. *J. Geophys. Res. Atmos.*, **120**, 6034–6055, https://doi.org/10.1002/2015JD023156.
Kollias, P., and B. Albrecht, 2010: Vertical velocity statistics in fair-weather cumuli at the ARM TWP Nauru Climate Research Facility. *J. Climate*, **23**, 6590–6604, https://doi.org/10.1175/2010JCLI3449.1.
——, R. Lhermitte, and B. Albrecht, 1999: Vertical air motion and raindrop size distributions in convective systems using a 94 GHz radar. *Geophys. Res. Lett.*, **26**, 3109–3112, https://doi.org/10.1029/1999GL010838.
——, B. Albrecht, and F. Marks Jr., 2002: Why Mie? *Bull. Amer. Meteor. Soc.*, **83**, 1471–1484, https://doi.org/10.1175/BAMS-83-10-1471.
——, ——, and ——, 2003: Cloud radar observations of vertical drafts and microphysics in convective rain. *J. Geophys. Res.*, **108**, 4053, https://doi.org/10.1029/2001JD002033.
——, ——, E. E. Clothiaux, M. A. Miller, K. L. Johnson, and K. P. Moran, 2005: The Atmospheric Radiation Measurement program cloud profiling radars: An evaluation of signal processing and sampling strategies. *J. Atmos. Oceanic Technol.*, **22**, 930–948, https://doi.org/10.1175/JTECH1749.1.
——, E. E. Clothiaux, M. A. Miller, B. A. Albrecht, G. L. Stephens, and T. P. Ackerman, 2007: Millimeter-wavelength radars: New frontier in atmospheric cloud and precipitation research. *Bull. Amer. Meteor. Soc.*, **88**, 1608–1624, https://doi.org/10.1175/BAMS-88-10-1608.
——, J. Rémillard, E. Luke, and W. Szyrmer, 2011: Cloud radar Doppler spectra in drizzling stratiform clouds: 1. Forward modeling and remote sensing applications. *J. Geophys. Res.*, **116**, D13201, https://doi.org/10.1029/2010JD015237.
——, N. Bharadwaj, K. Widener, I. Jo, and K. Johnson, 2014a: Scanning ARM cloud radars. Part I: Operational sampling strategies. *J. Atmos. Oceanic Technol.*, **31**, 569–582, https://doi.org/10.1175/JTECH-D-13-00044.1.
——, and Coauthors, 2014b: Scanning ARM cloud radars. Part II: Data quality control and processing. *J. Atmos. Oceanic Technol.*, **31**, 583–598, https://doi.org/10.1175/JTECH-D-13-00045.1.
——, S. Tanelli, A. Battaglia, and A. Tatarevic, 2014c: Evaluation of EarthCARE cloud profiling radar Doppler velocity measurements in particle sedimentation regimes. *J. Atmos. Oceanic Technol.*, **31**, 366–386, https://doi.org/10.1175/JTECH-D-11-00202.1.
——, and Coauthors, 2016: Development and applications of ARM millimeter-wavelength cloud radars. *The Atmospheric Radiation Measurement (ARM) Program: The First 20 Years*, *Meteor. Monogr.*, No. 57, Amer. Meteor. Soc., https://doi.org/10.1175/AMSMONOGRAPHS-D-15-0037.1.
——, A. Battaglia, A. Tatarevic, K. Lamer, F. Tridon, and L. Pfitzenmaier, 2018: The EarthCARE Cloud Profiling Radar (CPR) Doppler measurements in deep convection: Challenges, post-processing, and science applications. *Proc. SPIE*, **10776**, 107760R, https://doi.org/10.1117/12.2324321.
——, B. Puigdomènech Treserras, and A. Protat, 2019: Calibration of the 2007–2017 record of Atmospheric Radiation Measurements cloud radar observations using CloudSat. *Atmos. Meas. Tech.*, **12**, 4949–4964, https://doi.org/10.5194/AMT-12-4949-2019.
Küchler, N., S. Kneifel, P. Kollias, and U. Löhnert, 2018: Revisiting liquid water content retrievals in warm stratified clouds: The modified Frisch. *Geophys. Res. Lett.*, **45**, 9323–9330, https://doi.org/10.1029/2018GL079845.
Lamer, K., P. Kollias, and L. Nuijens, 2015: Observations of the variability of shallow trade wind cumulus cloudiness and mass flux. *J. Geophys. Res. Atmos.*, **120**, 6161–6178, https://doi.org/10.1002/2014JD022950.
——, A. M. Fridlind, A. S. Ackerman, P. Kollias, E. E. Clothiaux, and M. Kelley, 2018: $(GO)^2$-SIM: A GCM-oriented ground-observation forward-simulator framework for objective evaluation of cloud and precipitation phase. *Geosci. Model Dev.*, **11**, 4195–4214, https://doi.org/10.5194/gmd-11-4195-2018.
——, B. Puigdomènech Treserras, Z. Zhu, B. Isom, N. Bharadwaj, and P. Kollias, 2019: Characterization of shallow oceanic precipitation using profiling and scanning radar observations at the Eastern North Atlantic ARM observatory. *Atmos. Meas. Tech.*, **12**, 4931–4947, https://doi.org/10.5194/AMT-12-4931-2019.
Leinonen, J., and D. Moisseev, 2015: What do triple-frequency radar signatures reveal about aggregate snowflakes? *J. Geophys. Res. Atmos.*, **120**, 229–239, https://doi.org/10.1002/2014JD022072.
LeMone, M. A., and E. J. Zipser, 1980: Cumulonimbus vertical velocity events in GATE. Part I: Diameter, intensity and mass flux. *J. Atmos. Sci.*, **37**, 2444–2457, https://doi.org/10.1175/1520-0469(1980)037<2444:CVVEIG>2.0.CO;2.
Lhermitte, R. M., 1987: Small cumuli observed with a 3 mm wavelength Doppler radar. *Geophys. Res. Lett.*, **14**, 707–710, https://doi.org/10.1029/GL014i007p00707.
——, and L. J. Miller, 1970: Doppler radar methodology for the observation of convective storms. Preprints, *14th Radar Meteor. Conf.*, Tucson, AZ, Amer. Meteor. Soc., 133–138.
Li, H., and D. Moisseev, 2019: Melting layer attenuation at Ka- and W-bands as derived from multifrequency radar Doppler spectra observations. *J. Geophys. Res. Atmos.*, **124**, 9520–9533, https://doi.org/10.1029/2019JD030316.
Li, L., G. M. Heymsfield, L. Tian, and P. E. Racette, 2005: Measurements of ocean surface backscattering using an airborne 94-GHz cloud radar—Implication for calibration of airborne and spaceborne W-band radars. *J. Atmos. Oceanic Technol.*, **22**, 1033–1045, https://doi.org/10.1175/JTECH1722.1.
Luke, E. P., and P. Kollias, 2013: Separating cloud and drizzle radar moments during precipitation onset using Doppler spectra. *J. Atmos. Oceanic Technol.*, **30**, 1656–1671, https://doi.org/10.1175/JTECH-D-11-00195.1.
——, ——, K. L. Johnson, and E. E. Clothiaux, 2008: A technique for the automatic detection of insect clutter in cloud radar returns. *J. Atmos. Oceanic Technol.*, **25**, 1498–1513, https://doi.org/10.1175/2007JTECHA953.1.
——, ——, and M. D. Shupe, 2010: Detection of supercooled liquid in mixed-phase clouds using radar Doppler spectra. *J. Geophys. Res.*, **115**, D19201, https://doi.org/10.1029/2009JD012884.
Luo, Y., K.-M. Xu, H. Morrison, and G. McFarquhar, 2008: Arctic mixed-phase clouds simulated by a cloud-resolving model: Comparison with ARM observations and sensitivity to microphysics parameterizations. *J. Atmos. Sci.*, **65**, 1285–1303, https://doi.org/10.1175/2007JAS2467.1.
Maahn, M., 2015: Exploiting vertically pointing Doppler radar for advancing snow and ice cloud observations. Ph.D. dissertation, Universität zu Köln, 181 pp.
Martner, B. E., 1993: Cloud liquid water content measurement tests using dual-wavelength radar. NOAA Tech. Memo. ERL WPL-215, 47 pp.
Mather, J. H., and J. W. Voyles, 2013: The ARM Climate Research Facility: A review of structure and capabilities. *Bull. Amer. Meteor. Soc.*, **94**, 377–392, https://doi.org/10.1175/BAMS-D-11-00218.1.
Matrosov, S. Y., M. Maahn, and G. Boer, 2019: Observational and modeling study of ice hydrometeor radar dual-wavelength ratios. *J. Appl. Meteor. Climatol.*, **58**, 2005–2017, https://doi.org/10.1175/JAMC-D-19-0018.1.
Matsui, T., B. Dolan, S. A. Rutledge, W. K. Tao, T. Iguchi, J. Barnum, and S. E. Lang, 2019: POLARRIS: A Polarimetric Radar Retrieval and Instrument Simulator. *J. Geophys. Res. Atmos.*, **124**, 4634–4657, https://doi.org/10.1029/2018JD028317.
Moisseev, D. N., C. M. Unal, H. W. Russchenberg, and L. P. Ligthart, 2002: Improved polarimetric calibration for atmospheric radars. *J. Atmos. Oceanic Technol.*, **19**, 1968–1977, https://doi.org/10.1175/1520-0426(2002)019<1968:IPCFAR>2.0.CO;2.
Moran, K. P., B. E. Martner, M. Post, R. A. Kropfli, D. C. Welsh, and K. B. Widener, 1998: An unattended cloud-profiling radar for use in climate research. *Bull. Amer. Meteor.*

Soc., **79**, 443–455, https://doi.org/10.1175/1520-0477(1998)079<0443:AUCPRF>2.0.CO;2.

North, K. W., M. Oue, P. Kollias, S. E. Giangrande, S. M. Collis, and C. K. Potvin, 2017: Vertical air motion retrievals in deep convective clouds using the ARM scanning radar network in Oklahoma during MC3E. *Atmos. Meas. Tech.*, **10**, 2785–2806, https://doi.org/10.5194/AMT-10-2785-2017.

O'Connor, E. J., R. J. Hogan, and A. J. Illingworth, 2005: Retrieving stratocumulus drizzle parameters using Doppler radar and lidar. *J. Appl. Meteor.*, **44**, 14–27, https://doi.org/10.1175/JAM-2181.1.

Oue, M., M. R. Kumjian, Y. Lu, Z. Jiang, E. E. Clothiaux, J. Verlinde, and K. Aydin, 2015: X-band polarimetric and Ka-band Doppler spectral radar observations of a graupel-producing Arctic mixed-phase cloud. *J. Appl. Meteor. Climatol.*, **54**, 1335–1351, https://doi.org/10.1175/JAMC-D-14-0315.1.

——, P. Kollias, A. Ryzhkov, and E. P. Luke, 2018: Toward exploring the synergy between cloud radar polarimetry and Doppler spectral analysis in deep cold precipitating systems in the Arctic. *J. Geophys. Res. Atmos.*, **123**, 2797–2815, https://doi.org/10.1002/2017JD027717.

——, ——, A. Shapiro, A. Tatarevic, and T. Matsui, 2019: Investigation of observational error sources in multi-Doppler-radar three-dimensional variational vertical air motion retrievals. *Atmos. Meas. Tech.*, **12**, 1999–2018, https://doi.org/10.5194/amt-12-1999-2019.

——, A. Tatarevic, P. Kollias, D. Wang, K. Yu, and A. M. Vogelmann, 2020: The Cloud Resolving Model Radar Simulator (CR-SIM) version 3.2: Description and applications of a virtual observatory. *Geosci. Model Dev.*, **13**, 1975–1998, https://doi.org/10.5194/gmd-13-1975-2020.

Potvin, C. K., D. Betten, L. J. Wicker, K. L. Elmore, and M. I. Biggerstaff, 2012: 3DVAR versus traditional dual-Doppler wind retrievals of a simulated supercell thunderstorm. *Mon. Wea. Rev.*, **140**, 3487–3494, https://doi.org/10.1175/MWR-D-12-00063.1.

Protat, A., and I. Zawadzki, 1999: A variational method for real-time retrieval of three-dimensional wind field from multiple-Doppler bistatic radar network data. *J. Atmos. Oceanic Technol.*, **16**, 432–449, https://doi.org/10.1175/1520-0426(1999)016<0432:AVMFRT>2.0.CO;2.

——, D. Bouniol, E. O'Connor, H. Klein Baltink, J. Verlinde, and K. Widener, 2011: *CloudSat* as a global radar calibrator. *J. Atmos. Oceanic Technol.*, **28**, 445–452, https://doi.org/10.1175/2010JTECHA1443.1.

Rambukkange, M. P., J. Verlinde, E. W. Eloranta, C. J. Flynn, and E. E. Clothiaux, 2011: Using Doppler spectra to separate hydrometeor populations and analyze ice precipitation in multilayered mixed-phase clouds. *IEEE Geosci. Remote Sens. Lett.*, **8**, 108–112, https://doi.org/10.1109/LGRS.2010.2052781.

Rémillard, J., and Coauthors, 2017: Use of cloud radar Doppler spectra to evaluate stratocumulus drizzle size distributions in large-eddy simulations with size-resolved microphysics. *J. Appl. Meteor. Climatol.*, **56**, 3263–3283, https://doi.org/10.1175/JAMC-D-17-0100.1.

Ryzhkov, A., P. Zhang, H. Reeves, M. Kumjian, T. Tschallener, S. Trömel, and C. Simmer, 2016: Quasi-vertical profiles—A new way to look at polarimetric radar data. *J. Atmos. Oceanic Technol.*, **33**, 551–562, https://doi.org/10.1175/JTECH-D-15-0020.1.

Schiro, K. A., and J. D. Neelin, 2018: Tropical continental downdraft characteristics: Mesoscale systems versus unorganized convection. *Atmos. Chem. Phys.*, **18**, 1997–2010, https://doi.org/10.5194/acp-18-1997-2018.

——, F. Ahmed, S. E. Giangrande, and J. D. Neelin, 2018: GoAmazon2014/5 campaign points to deep-inflow approach to deep convection across scales. *Proc. Natl. Acad. Sci. USA*, **115**, 4577–4582, https://doi.org/10.1073/pnas.1719842115.

Shupe, M. D., 2007: A ground-based multisensor cloud phase classifier. *Geophys. Res. Lett.*, **34**, L22809, https://doi.org/10.1029/2007GL031008.

——, P. Kollias, S. Y. Matrosov, and T. L. Schneider, 2004: Deriving mixed-phase cloud properties from Doppler radar spectra. *J. Atmos. Oceanic Technol.*, **21**, 660–670, https://doi.org/10.1175/1520-0426(2004)021<0660:DMCPFD>2.0.CO;2.

——, and Coauthors, 2008: A focus on mixed-phase clouds: The status of ground-based observational methods. *Bull. Amer. Meteor. Soc.*, **89**, 1549–1562, https://doi.org/10.1175/2008BAMS2378.1.

Song, H., W. Lin, Y. Lin, A. B. Wolf, R. Neggers, L. J. Donner, A. D. Del Genio, and Y. Liu, 2013: Evaluation of precipitation simulated by seven SCMs against the ARM observations at the SGP site. *J. Climate*, **26**, 5467–5492, https://doi.org/10.1175/JCLI-D-12-00263.1.

——, and Coauthors, 2014: Evaluation of cloud fraction simulated by seven SCMs against the ARM observations at the SGP site. *J. Climate*, **27**, 6698–6719, https://doi.org/10.1175/JCLI-D-13-00555.1.

Tanelli, S., S. L. Durden, E. Im, K. S. Pak, D. G. Reinke, P. Partain, J. M. Haynes, and R. T. Marchand, 2008: CloudSat's cloud profiling radar after two years in orbit: Performance, calibration, and processing. *IEEE Trans. Geosci. Remote Sens.*, **46**, 3560–3573, https://doi.org/10.1109/TGRS.2008.2002030.

Tridon, F., and A. Battaglia, 2015: Dual-frequency radar Doppler spectral retrieval of rain drop size distributions and entangled dynamics variables. *J. Geophys. Res. Atmos.*, **120**, 5585–5601, https://doi.org/10.1002/2014jd023023.

——, ——, and P. Kollias, 2013: Disentangling Mie and attenuation effects in rain using a Ka-W dual-wavelength Doppler spectral ratio technique. *Geophys. Res. Lett.*, **40**, 5548–5552, https://doi.org/10.1002/2013GL057454.

Turner, D. D., S. A. Clough, J. C. Liljegren, E. E. Clothiaux, K. E. Cady-Pereira, and K. L. Gaustad, 2007: Retrieving liquid water path and precipitable water vapor from the Atmospheric Radiation Measurement (ARM) microwave radiometers. *IEEE Trans. Geosci. Remote Sens.*, **45**, 3680–3690, https://doi.org/10.1109/TGRS.2007.903703.

van Diedenhoven, B., A. Fridlind, A. Ackerman, E. Eloranta, and G. McFarquhar, 2009: An evaluation of ice formation in large-eddy simulations of supercooled Arctic stratocumulus using ground-based lidar and cloud radar. *J. Geophys. Res.*, **114**, D10203, https://doi.org/10.1029/2008JD011198.

Varble, A., and Coauthors, 2014: Evaluation of cloud-resolving and limited area model intercomparison simulations using TWP-ICE observations: 1. Deep convective updraft properties. *J. Geophys. Res. Atmos.*, **119**, 13 891–13 918, https://doi.org/10.1002/2013JD021371.

Vivekanandan, J., D. S. Zrnić, S. M. Ellis, R. Oye, A. V. Ryzhkov, and J. Straka, 1999: Cloud microphysics retrieval using S-band dual-polarization radar measurements. *Bull. Amer. Meteor. Soc.*, **80**, 381–388, https://doi.org/10.1175/1520-0477(1999)080<0381:CMRUSB>2.0.CO;2.

Yoshida, Y., S. Asano, and K. Iwanami, 2006: Retrieval of microphysical properties of water, ice, and mixed-phase clouds using a triple-wavelength radar and microwave radiometer. *J. Meteor. Soc. Japan*, **84**, 1005–1031, https://doi.org/10.2151/JMSJ.84.1005.

Yu, G., J. Verlinde, E. E. Clothiaux, and Y.-S. Chen, 2014: Mixed-phase cloud phase partitioning using millimeter wavelength cloud radar Doppler velocity spectra. *J. Geophys. Res. Atmos.*, **119**, 7556–7576, https://doi.org/10.1002/2013JD021182.

Zeng, X., and Coauthors, 2007: Evaluating clouds in long-term cloud-resolving model simulations with observational data. *J. Atmos. Sci.*, **64**, 4153–4177, https://doi.org/10.1175/2007JAS2170.1.

Zhang, Y., and Coauthors, 2018: The ARM cloud radar simulator for global climate models: Bridging field data and climate models. *Bull. Amer. Meteor. Soc.*, **99**, 21–26, https://doi.org/10.1175/BAMS-D-16-0258.1.

Zhu, Z., K. Lamer, P. Kollias, and E. E. Clothiaux, 2019: The vertical structure of liquid water content in shallow clouds as retrieved from dual-wavelength radar observations. *J. Geophys. Res. Atmos.*, **124**, 14 184–14 197, https://doi.org/10.1029/2019JD031188.